Polarforschung 60 (1): 25–32, 1990 (erschienen 1991)

Melting Rates at the Bottom of Filchner-Ronne Ice Shelf, Antarctica, from Short-term Mass-balance Studies

By Jürgen Determann*, Klaus Grosfeld** and Bernhard Ritter***

Summary: Field studies which were performed in 1990 on a strain network yielded all quantities which are necessary to solve the mass-conservation equation with respect to the melting rate underneath the Filchner-Ronne Ice Shelf, Antarctica. The network was located about 30 km inland from the ice front and about 50 km north-west of Filchner Station. Repeated electro-optical distance measurements, direction observations and absolut positioning using satellite methods (GPS), determined strain rates and ice-flow velocities. Ice thickness and ice-thickness gradients were obtained by hot-water drilling and electro-magnetic reflection soundings (EMR), respectively. Surface accumulation rates were taken from measurements in snow pits. Due to the high precision of the used field techniques, about one month between re-observations was sufficient to estimate a melting rate of 1.5 m/a within 0.15 m/a of accuracy.

Zusammenfassung: Das vorgestellte Feldexperiment liefert die in die Kontinuitätsgleichung für den Massenfluß eingehenden Größen, so daß, unter Annahme eines stationären Schelfeises daraus die Schmelzrate zu berechnen ist. Die in die Rechnung eingehenden Daten über Figur und Dynamik des Filchner-Ronne Schelfeises wurden 1990 innerhalb einer Deformationsfigur gewonnen. Die Lokation befand sich etwa 30 km landeinwärts der Schelfeiskante und ca. 50 km
nordwestlich der Filchner-Station. Eismächtigkeiten und deren laterale Gradienten sind mit dem Elektromagnetischen Reflektionsverfahren (EMR) zu gewinnen. Satelliten-Positionierungsverfahren und Laser-Entfernungsmessungen liefern Betrag und Richtung der Fließgeschwindigkeit sowie die Deformationsraten des Schelfeises. Glaziologische Untersuchungen ergeben Beträge der jährlichen Zutragsraten durch Schneefall.
Die Kombination präziser geodätischer und geophysikalischer Meßmethoden in Verbindung mit einer geeigneten Dimensionierung der Deformationsfigur ermöglicht bereits nach einem Beobachtungsintervall von 4 Wochen, genaue Aussagen über die Schmelzraten zu machen. Für den genannten Bereich ergibt sich eine Schmelzrate von 1,5 m/Jahr mit einem Meßfehler von weniger als 0,15 m/Jahr.

INTRODUCTION

Climatic concerns recommend the investigation of the equilibrium state of the Antarctic Ice Sheet. Therefore the entire mass budget has to be evaluated. Floating ice shelves which drain most of the annual precipitation accumulating on the continent (roughly 2000 km³/a, BUDD & SMITH 1985), appeared to be suitable areas for monitoring outflowing ice masses. In addition to a loss by calving of icebergs, melting at the ice-shelf bottom recently gained attention among researchers (e.g. DOAKE 1985). Unlike calving rates which can be obtained by measuring the horizontal advection of ice across a reference line, bottom melting rates cannot yet be measured directly. Melting rates can be derived by calculating the terms of the mass-conservation equation. The high variation in extent and magnitude of melting rates to be expected underneath ice shelves may become obvious by comparing some previous findings. For different locations close to the ice shelf front BERENDT (1970) and KOHNEN (1982) derived melting rates of 9 m/a and 3 m/a, respectively. Recently, JENKINS & DOAKE (1991) found magnitudes of 4 m/a next to the grounding line where Rutford ice stream feeds into the Filchner-Ronne Ice Shelf (FRIS).

In order to gain additional information on the spatial variation of the melting rate underneath FRIS, we introduce an experiment yieding data to calculate this quantity from short-term mass-balance studies within a single field season. The field studies were carried out during the German Antarctic Expedition (ANT-VIII) 1989/90 to FRIS (Fig. 1).

THEORY

A basic assumption to perform mass-balance calculations is to treat ice as an incompressible medium. Then the theory of continuum mechanics leads to the following equation:

* Dr. Jürgen Determann, Alfred-Wegener-Institut für Polar- und Meeresforschung, Columbusstr., D-2850 Bremerhaven
** Klaus Grosfeld, Forschungsstelle für physikalische Glaziologie, Universität Münster, Correnssstr. 24, D-4400 Münster.
*** Dr. Bernhard Ritter, Institut für Vermessungskunde, Technische Universität Braunschweig, Pockelsstr. 4, D-3300 Braunschweig.
Manuscript received 19 March 1991, accepted 5 June 1991.

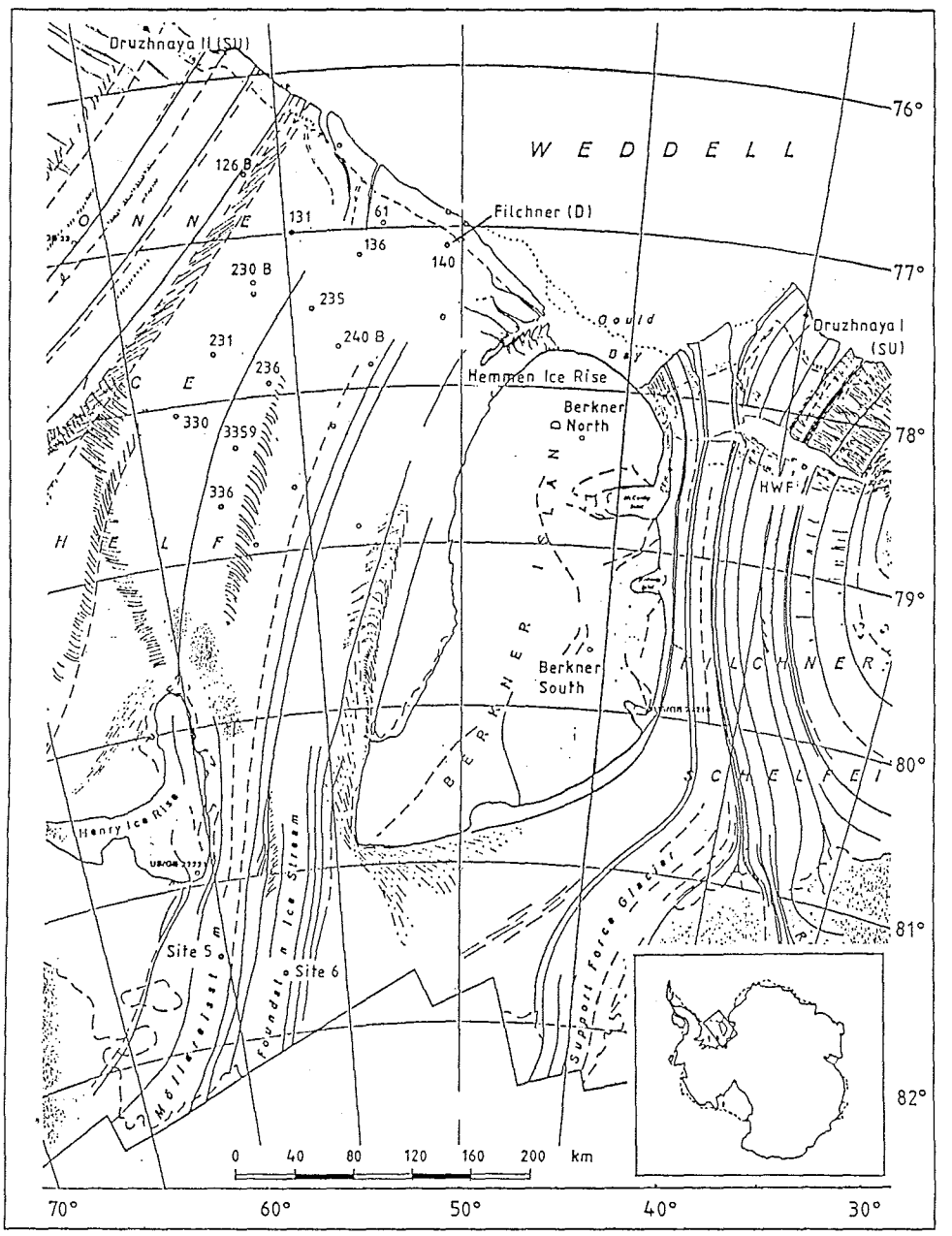

Fig. 1: The Filchner-Ronne Ice shelf (FRIS) and its relation to the Antarctic Ice Sheet (extracted from SWITHINBANK et al. 1988). Surveying was carried out on a strain network next to site 61 about 50 km north-west of Filchner Station (140).

Abb. 1: Das Filchner-Ronne Schelfeis (FRIS) und seine relative Lage zum antarktischen Kontinent (aus SWITHINBANK et al. 1988). Die Beobachtungen wurden in einer Deformationsfigur nahe Punkt 61 etwa 50 km nordwestlich der Filchner Station (140) durchgeführt.

$$\varepsilon_{xx} + \varepsilon_{yy} = - \varepsilon_{zz} \quad (1)$$

saying that horizontal strain rates ε_{xx} and ε_{yy} are balanced by the vertical strain rate ε_{zz}. It might be objected that this does not hold for an ice shelf and its upper compressible firn layer of perhaps 50 m thickness. But, if we assume this firn layer to be laterally homogeneous on small scales, eq. (1) is approximately valid. After having expressed strain rates in terms of velocity gradients according to: $\varepsilon_{ii}=\partial u_i/\partial x_i$, integration of (1) with respect to the vertical co-ordinate from the ice-shelf bottom to the surface yields the continuity equation for mass conservation.

$$\partial H/\partial t = - \partial/\partial x(Hu) - \partial/\partial y(Hv) + a - m \quad (2)$$

This formula which has been taken for granted widely in glaciology (e.g. CRARY et al. 1962) leads to transient changes of ice thickness H by calculating the divergence of the vertically integrated ice flux (Hu, Hv), and by adding surface accumulation a and bottom melting m. u and v are the horizontal components of the ice-flow vector U which is constant with depth due to lack of shear forces at the ice-shelf bottom (SANDERSON & DOAKE 1979). If we assume the ice shelf to be in steady state ($\partial H/\partial t = 0$), the melting rate can be calculated according to:

$$m = -\partial/\partial x(Hu) - \partial/\partial y(Hv) + a \quad (3)$$

Working out this equation, one can easily see that it is equivalent to

$$m = -u\partial H/\partial x - v\partial H/\partial y + H\varepsilon_{zz} + a \quad (4)$$

Thus, we can calculate bottom melting rates m by quantities which have to be derived from measurements at the ice-shelf surface.

METHODS AND RESULTS

All quantities necessary to solve (4) were obtained on a strain network which was located about 30 km inland from the ice front of FRIS and about 50 km north-west of Filchner Station (Fig. 1). The strain network (Fig. 2) contained two main axes of 10 km length each, one of which was directed almost parallel to the observed ice-shelf flow vector (RITTER & KARSTEN 1991). The second axis crossed the first one at km 7.5 (point 4) right-

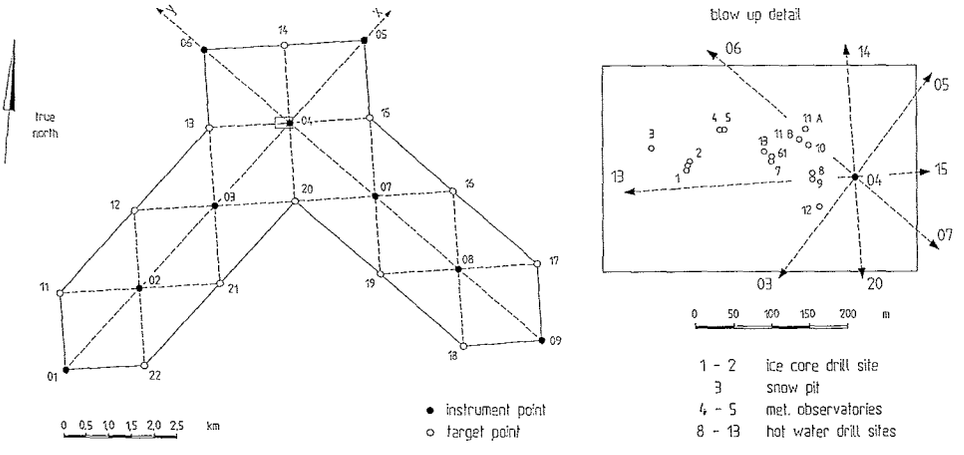

Fig. 2: 24 triangles are arranged to a network which has two main axes of 10 km length each. The x axis is almost parallel to the observed ice-flow vector U.

Abb. 2: 24 Dreiecke bilden eine Deformationsfigur mit zwei Hauptachsen von jeweils 10 km Länge. Die x-Achse liegt etwa parallel zur beobachteten Fließrichtung U des Eises.

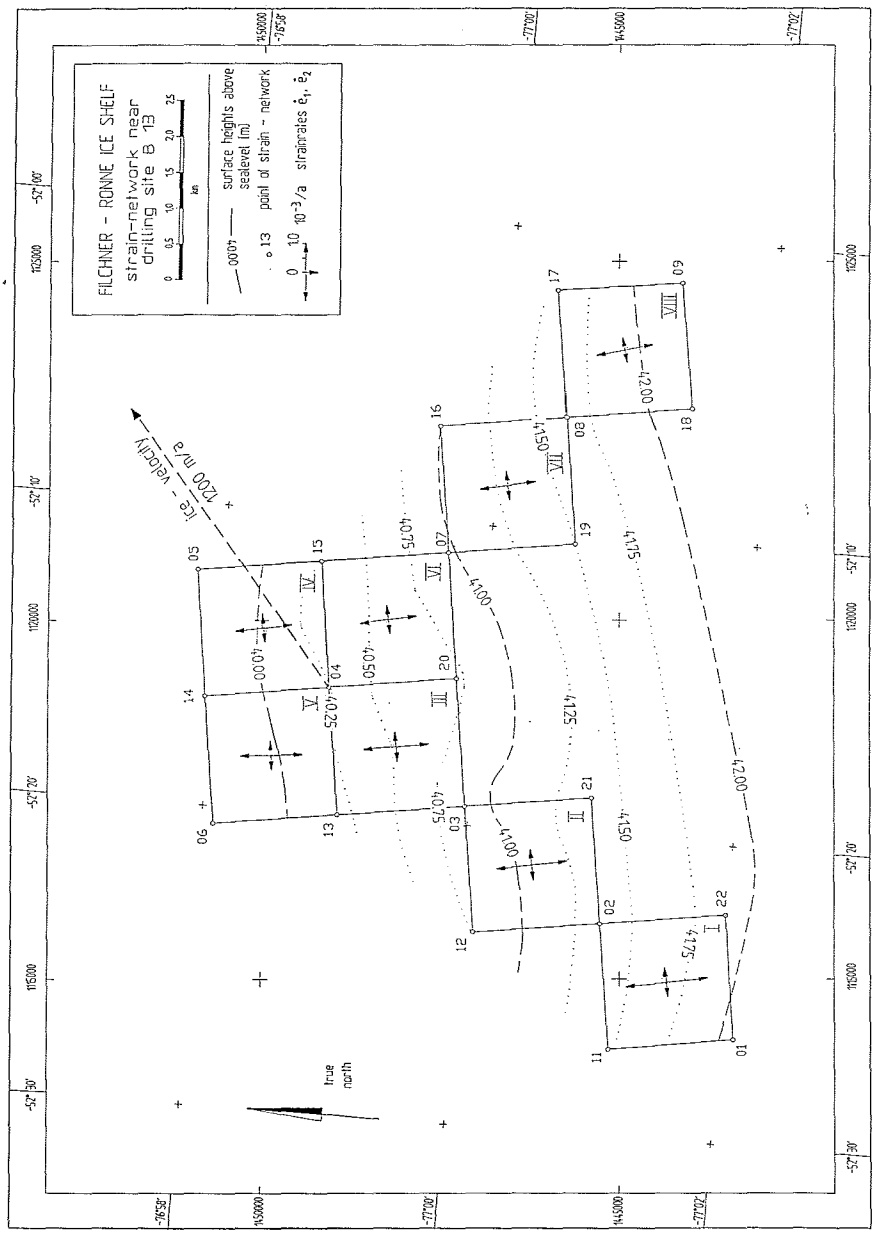

Fig. 3: Horizontal strain rates for 8 squares within the network. Stretching in both directions implies ice-shelf thinning ($\dot{e}_{1,2} < 0$). The principal strain rate $\dot{e}_1$ points towards the steepest descent of ice thicknesses which is indicated by contour lines of surface altitudes. A vector at point 4 indicates the ice-flow direction.

Abb. 3: Horizontale Deformationsraten für acht Quadrate innerhalb der Deformationsfigur. Eine Ausdehnung in beide Richtungen deutet eine Ausdünnung des Schelfeises an ($\dot{e}_{1,2} < 0$). Die maximale Komponente der Deformation $\dot{e}_1$ weist in Richtung der größten Neigung der Eisoberfläche, angedeutet durch Höhenlinien. Ein Vektor an Punkt 4 zeigt die Fließrichtung des Eises an.

location	$\dot{\varepsilon}_{zz}$ [$10^{-3}a^{-1}$]	H [m]
I	- 1.94	254.5
II	- 1.79	249.5
III	- 1.64	243.5
IV	- 1.49	239.5
V	- 1.60	234.5
VI	- 1.55	242.0
VII	- 1.48	246.5
VIII	- 1.46	251.5

Tab. 1: Vertical strain rates and ice thicknesses at the centres of 8 squares within the network (Fig. 3); therefrom thinning due to ice-shelf spreading is calculated to be of the order of 0.4 m/a ($\sigma < 0.05$ m/a)

Tab. 1: Vertikale Deformationsraten und Eismächtigkeiten für acht Quadrate innerhalb der Deformationsfigur; danach bewirkt das Fließen des Eises eine Ausdünnung von 0,4 m/a ($\sigma<0,05$ m/a)

angled. The intersection point was close to a hot-water drill site, where the ice shelf was found to be 239 m (+/- 2m) thick (GROSFELD 1990). The axis connecting point 1 and 5 of the network was chosen to be the x axis in the system. Respectively, point 9 and 6 defined the y axis.

38 slope distances within the network ranging from 1750 to 2500 m, have been measured using a KERN ME 5000 laser distance-measuring equipment. Standard deviations σ of less than 2.5 mm express the high precision of this method. Further, observation of horizontal directions and zenith angles led to a calculation of reliable co-ordinates within the network. Principal strain rates $\varepsilon_1,\varepsilon_2$ due to ice-shelf spreading have been calculated in 24 triangles from two sets of co-ordinates which were re-evaluated after 25 days of deformation. Since eq. (1) is invariant with respect to co-ordinate transformations, the sum of $\varepsilon_1,\varepsilon_2$ equals that of $\varepsilon_{xx},\varepsilon_{yy}$. ε_1 points towards the direction of maximum strain while e_2 is perpendicular to e_1. Standard deviations for the strain rates were estimated to be less than 0.08 x 10^{-3} a^{-1} (triangles). Calculated vertical strain rates e_{zz} (= - ε_1 - ε_2) for 8 squares within the

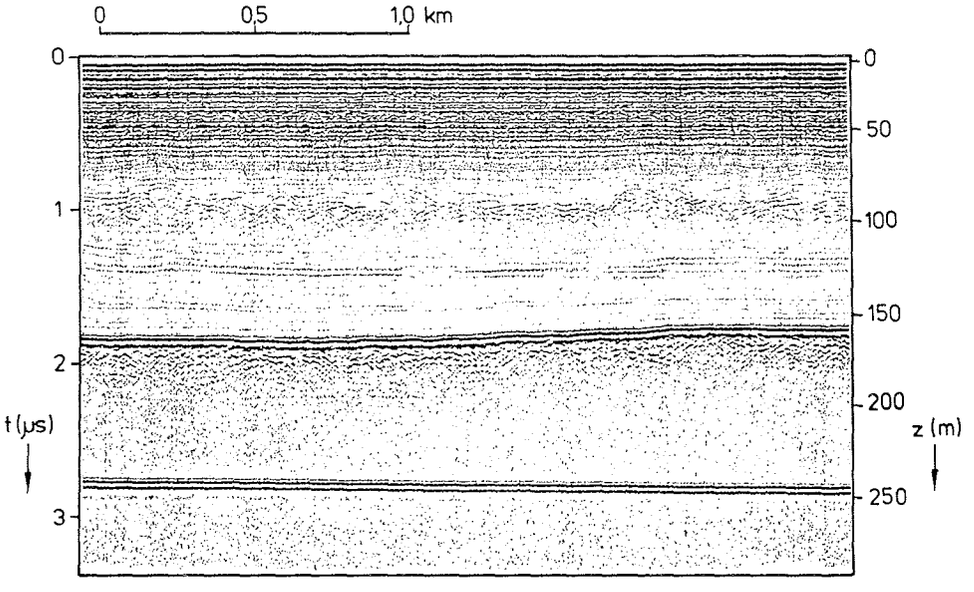

Fig. 4: Example for continuous EMR profiling between points 4 and 5 of the strain network showing prominent reflections from the meteoric/ marine ice transition zone (1.8 μs), and from the ice-shelf bottom (2.7 μs).

Abb. 4: Das Beispiel einer kontinuierlichen EMR Kartierung zwischen Punkt 4 und 5 der Deformationsfigur zeigt deutliche Reflektionen von der Übergangszone zwischen meteorischem und marinen Eis (1,8 μs), sowie von der Eisunterseite (2,7 μs).

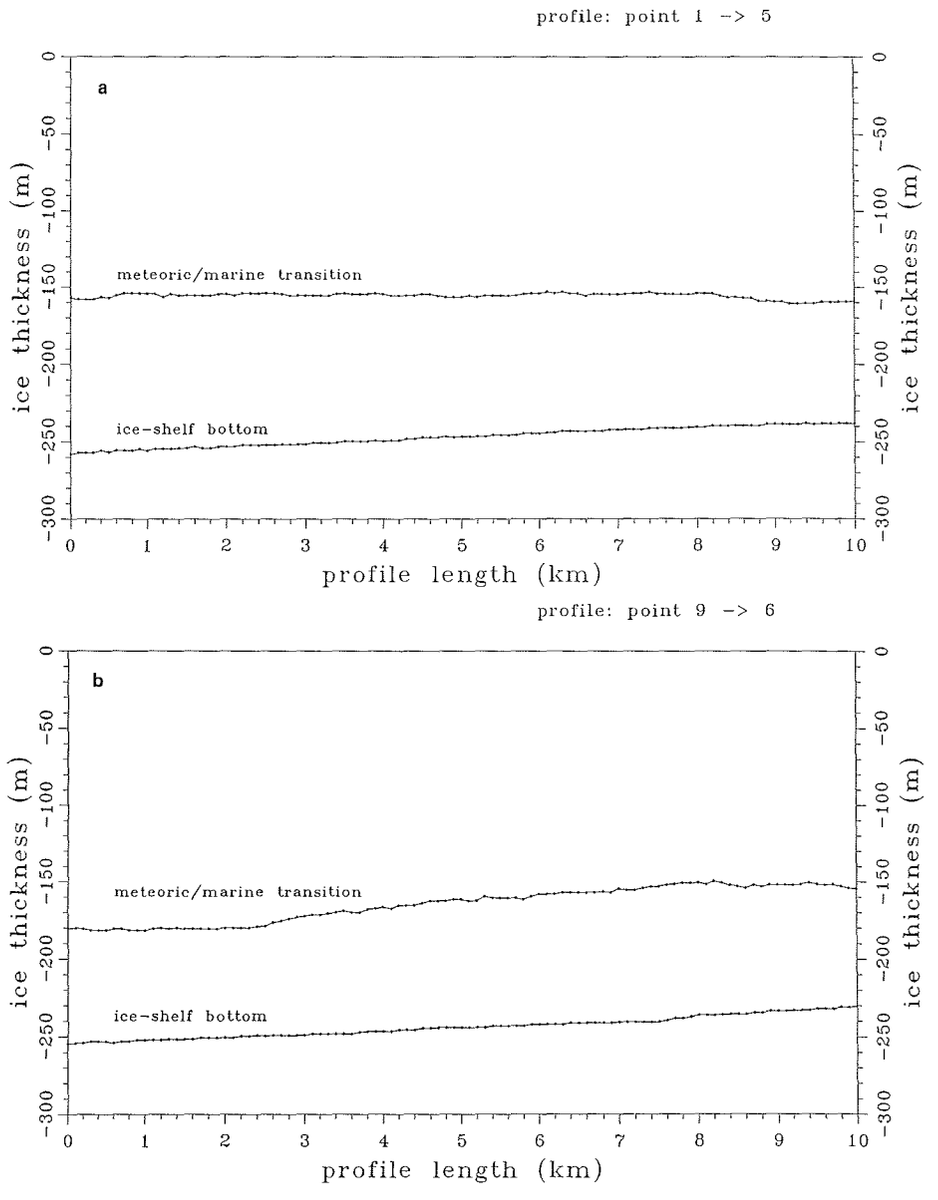

Fig. 5: Ice-thickness profiles as derived from EMR soundings. Ice thicknesses decrease in x direction by 20 m a), and b) y direction by 24 m.

Abb. 5: Profile der Eisdicken aus EMR Messungen. Die Eismächtigkeiten nehmen a) in x-Richtung um 20 m ab, b) in y-Richtung um 24 m ab.

network (Fig. 4; Tab 1) show even less uncertainties ($\sigma < 0.06 \times 10^{-3}\ a^{-1}$). The principal strain rate $\dot{\varepsilon}_1$ points towards the steepest descent of the surface elevation which was derived from trigonometric levelling.

As the lateral change in mass flux is the most important term for the calculation of the melting rate by means of eq. (4), much effort was spent on measuring the ice-shelf flow velocity. This was done using a Wild Magnavox WM 102 GPS receiver on point 61, which was close to the central point 5 (Fig. 2). From two extended sets of 8 positionings (sessions) each, two sets of absolut co-ordinates (latitude, longitude, ellipsoidic height) were

determined, yielding a horizontal displacement of 82,1 m within 25 days. Therefrom the flow velocity at the central point is estimated to be 1200 m/a (σ < 55 m/a). The azimuth of the flow direction is 49.45° (σ < 2°). Compared with the x-axis which has an azimuth of 36.5°, the ice-flow direction is about 13°. This leads to velocity components of 1170 m/a with respect to x, and of -269 m/a with respect to y.

Ice-shelf thickness has been investigated by high resolution electromagnetic reflection measurements. The measurements were performed with a 35 MHz monopulse sounder (BLINDOW 1986) and a constant offset between transmitting and receiving antennas. Continuous profiling was carried out along the major axis of the strain network with a sounding distance of about 1.5 m. Figure 4 shows an example of an EMR profile spanning a horizontal distance of 2.5 km. The first 0.5 µs are characterized by reflections mainly caused by density changes in the firn layering. The strong reflector at about 1.8 µs of travel time indicates the transition from meteoric to marine ice which is formed about 200 km further inland by accumulation of marine ice (THYSSEN 1988). The reflection from the ice-shelf bottom occurs at about 2.7 µs. Taking a velocity with depth function, derived from a common midpoint gather (CMP) at point 4 of the network (BLINDOW 1991), ice thickness H and the depth of the transition zone can be calculated from reflection travel times with respect to the ice surface. This determination was carried out every 100 m along the x and y axes with an accuracy of 0.5 m for dH and of better than 2 m for H.

As seen in Figure 5, ice thicknesses decrease in both, x and y directions by about 20 m and 24 m, respectively. This already implies a substantial melting rate in the investigated site because thinning due to spreading is almost balanced by the surface accumulation rate of 0.25 m/a ice equivalent (GRAF et al. 1988). Though observed vertical strain rate magnitudes vary from -1.4 to -1.9 x 10^{-3} a^{-1}, we computed merely an average thinning rate of 0.4 m/a. All attempts at resolving a lateral trend in the melting rate failed due to the limited accuracy in dH. Small variations in the ice thickness on length scales of 2.5 km, for example, may arise from small-scale pertubations in the firn layer consistency. However, taking thickness gradients on these scales would imply decreasing melting rates on approaching the ice-shelf edge. Under the assumption that small-scale pertubations average out on greater scales, ice-thickness gradients were calculated on the full profile distance of 10 km yielding values of - 2.0 x 10^{-3} with respect to x and of - 2.4 x 10^{-3} with respect to y.

Summing up the terms of equation (4) (Tab. 2), the overall melting rate is 1.5 m/a (σ < 0.15m/a). The error bars emerge from calculation of Gaussian error propagation.

CONCLUSIONS

Field studies in remote areas like Filchner-Ronne Ice Shelf require extensive logistic and financial efforts. In order to optimize the data output (to obtain reasonable melting rates), we designed a field experiment requiring only a single field season to be completed. Since the flow velocity is the most crucial parameter in calculating melting rates, GPS location studies will define the lower time scale for observations as long as GPS differential mode positioning with respect to fixpoints cannot be used. In other words, we have to operate the receiver on a time scale that is sufficient to measure the flow velocity within about 5 % of accuracy. On the other hand, we can reduce efforts on determining strain rates because their contribution to the mass-balance calculation is of

term	magnitude	σ
dHx	20 m	0.5 m
dHy	24 m	0.5 m
u	1170 m/a	55 m/a
v	- 269 m/a	55 m/a
$\varepsilon_{zz}H$	- 0.4 m/a	0.05 m/a
a	0.25 m/a	0.05 m/a

Tab. 2: List of finally processed data which enter into equation (4).

Tab. 2: Liste der endgültig bearbeiteten Daten der in Gleichung (4) eingehenden Größen.

lower order. Hence, a more simple strain network could help to save time in favour of a higher quantity in the scientific output, like covering a larger area. This also holds for hot-water drilling which is known to be time as well as man-power consuming. Presently, sophisticated EMR techniques yield absolut ice thicknesses H within 2 m of accuracy which is more than sufficient to provide convincing results.

Our efforts were focussed primarily on the technique rather than gaining knowledge of the mass balance of the Antarctic Ice Sheet. Nevertheless, the method we introduced will provide a good tool to measure the contribution of ice shelves to the mass budget by bottom melting.

Though ice shelves are assumed to be close to a steady state (VAN DER VEEN 1986), neglecting transient ice-thickness changes is a major constraint in our theory. However, if *in situ* measurements of bottom melting, like those proposed by GROSFELD (1990), will gain definite ablation rates under ice shelves in future, then statements on their factual equilibrium state are possible. This would require hot-water drilling but it also would help to answer a major question of Antarctic glaciology.

ACKNOWLEDGEMENTS

Funding by the Deutsche Forschungsgemeinschaft (DFG) is gratefully acknowledged. Thanks are due to L. Hempel, A. Karsten and J. Kipfstuhl for their helpful assistance in the field work. This is contribution No. 423 of the Alfred Wegener Institute for Polar and Marine Research.

References

Berendt, J. C. (1970): The structure of the Filchner Ice Shelf and its relation to bottom melting.- ISAGE, Hannover Sept. 3-7, 1968, IASH Publ. No. 86: 488-496.

Budd, W. F. & Smith, I.N. (1985): The state of balance of the Antarctic Ice Sheet: an updated assesment 1984.- In: Glaciers, ice sheets and sea level: effect of a CO_2 induced climatic change, US Department of Energy, 172-177.

Blindow, N. (1986): Bestimmung der Mächtigkeit und des inneren Aufbaus von Schelfeis und temperierten Gletschern mit dem hochauflösenden elektromagnetischen Reflektionsverfahren.- Unpubl. Dissertation, Westfälische Wilhelms-Universität Münster, 164 pp.

Blindow, N. (1991): Structural features in the central part of the Filchner-Ronne Ice Shelf, Antarctica. – In: H. Miller & H. Oerter, eds., Filchner-Ronne Ice Shelf Programme Report 5, 12, Alfred Wegener Institute Polar and Marine Research, Bremerhaven.

Crary, A. P., Robinson, E.S., Bennet, M.F. & Boyd, W.W. jr. (1962): Glaciological regime of the Ross Ice Shelf.- J. Geophys. Res. 67 (7): 2791-2807.

Doake, C.S.M. (1985): Antarctic mass balance: glaciological evidence from Antarctic Peninsula and Weddell Sea sectors.- In: Glaciers, ice sheets and sea level: effect of a CO_2 induced climatic change. US Department of Energy, Washington, 197-209.

Graf, W., Moser, H, Oerter, H., Reinwarth, O. & Stichler, W. (1988): Accumulation and ice-core studies on Filchner-Ronne Ice Shelf, Antarctica.- Ann. Glaciol. 11: 23-31.

Grosfeld, K. (1990): Temperature profiles and investigation of the ice shelf/ocean boundary using hot water drilled holes: report of fieldwork on FRIS 1989/90.- In: Miller, H., ed., Filchner-Ronne Ice Shelf Programme Report 4, Alfred Wegener Institute for Polar and Marine Research, 109-111, Bremerhaven.

Kohnen, H. (1982): Glaciological investigations in the frontal zone of the Filchner and Ronne ice shelves.- Ann. Glaciol.,3: 160-165.

Jenkins, A. & Doake, C.S.M. (1991): Ice-ocean interaction on Ronne Ice Shelf, Antarctica.- J. Geophys. Res. 96 (C1): 791-813.

Ritter, B. & Karsten, A. (1991): Geodätische Arbeiten während der Antarktisexpedition 1989/90.- Ber. Polarforschung, 86, Bremerhaven.

Sanderson, T.J.O. & Doake, C.S.M. (1979): Is vertical shear in an ice shelf negligible?- J. Glaciol. 22(87): 285-292.

Swithinbank, C., Brunk, K. & Sievers, J. (1988). A glaciological map of Filchner-Ronne Ice Shelf, Antarctica.- Ann. Glaciol. 11: 150-155.

Thyssen, F. (1988): Special aspects of the central part of the Filchner-Ronne Ice Shelf, Antarctica.- Ann. Glaciol. 11: 173-179.

Van der Veen, J. C. (1986): Numerical modelling of ice shelves and ice tongues.- Ann. Geophysicae 4(B 1): 45-54.